Biodesign

pISSN 2288-6982 | eISSN 2288-7105

MINI REVIEW P 23-27

# Crystallization and preliminary X-ray diffraction analysis of a toxin-antitoxin MazEF complex from the extremophile *Deinococcus radiodurans*

**Immanuel Dhanasingh[1], Eunsil Choi[2], Jihwan Hwang[2] and Sung Haeng Lee[1]***

[1]Department of Cellular and Molecular Medicine, Chosun University School of Medicine, Gwangju 501-759, Korea, [2]Department of Microbiology, Pusan National University, Busan 46241, Korea

*Correspondence: sunglee@chosun.ac.kr

**Toxin–antitoxin (TA) systems are ubiquitous among most of prokaryotes and govern the cell death or growth arrest in response to environmental cues. TA systems are associated with adaptation of pathogens to unfavorable environments, indicating their potential as a target for antibiotics. Here, we purified and crystallized the TA complex from the extremophile *Deinococcus radiodurans*. The TA complex (DrMazEF) was co-expressed and pulled using the N-terminal glutathione S-transferase-tagged DrMazF. The complex was crystallized in 100 mM citric acid pH 3.5 containing 25% PEG3350. The crystal diffracted X-ray to a 2.6 Å resolution and belonged to the space group $P2_12_12_1$, with the unit cell parameters *a* = 46.01, *b* = 74.04, and *c* = 138.26 Å. The asymmetric unit of the crystal had six molecules in two heterotrimeric complexes with a calculated Mathew's coefficient of 1.84 $Å^3$ $Da^{-1}$ and a solvent content of 33.18%.**

## INTRODUCTION

Toxin-Antitoxin (TA) systems that are responsible for cell growth arrest and possibly cell death is ubiquitous among bacteria and archaea (Makarova et al., 2009). Each TA system consists of two proteins, namely a stable toxin protein and an unstable antidote antitoxin protein. The antitoxin neutralizes the toxin by forming a protein complex with the toxin (Kamada et al., 2003). Because of the labile nature of antitoxin, it is degraded by cellular proteases and must be replenished constantly. TA modules play roles in multiple processes from plasmid stabilization to apoptosis (Aizenman et al., 1996). Toxin proteins inhibit bacterial growth in several ways, by including the impairment of DNA replication, cell wall synthesis, translation, cell division and ATP production (Aakre et al., 2013). They are activated under adverse conditions such as starvation, antibiotic pressure, high temperatures, DNA damage and oxidative stress (Gerdes, Christensen et al. 2005, Nariya and Inouye 2008, Wang and Wood 2011).

*Eschesichia coli* has at least 34 TA systems. Interestingly, the pathogenic *Mycobacterium tuberculosis* has 70 TA systems, while its closest related non-pathogenic strain has only two TA systems, indicating the importance of TA systems in bacterial pathogenesis (Pandey and Gerdes 2005). TA systems are not essential for the normal growth of bacterial cells; however, their high prevalence indicates that they may provide advantages for bacterial survival under conditions of stress. Under the sudden onset of stress, toxins may promote bacterial adaptation by slowing down cell growth or causing some cells to die as in the case of fruiting body formation in *Myxococcus xanthus* (Nariya and Inouye, 2008). Once the stress is relieved, the remaining subpopulation becomes the seed for repopulation. Thus TA systems play a crucial role in the survival of bacteria upon the onset of any environmental stress, including antibiotic treatment.

The *maz*EF operon was the first TA system found in *E. coli* and many other bacteria, indicating that TA systems appear to have co-evolved (Aizenman et al., 1996, Kamada et al., 2003, Yamaguchi, Park et al. 2011). The MazEF family proteins comprise the MazE antitoxin (9 kDa) and the MazF (12kDa) toxin, which are homologous to the *kis/kid* TA module of *E.coli* plasmid R1 and the chromosomal *chp*BIK TA system (Tsuchimoto et al., 1988, Masuda et al., 1993). MazE and MazF form a linear heterohexamer complex composed of alternating toxin-antitoxin homodimers (2MazF-2MazE-2MazF) (Kamada et al., 2003). The toxin, MazF, is a sequence-specific endoribonuclease that cleaves cellular RNAs at 5′-ACA-3′ sites (Kamphuis et al., 2006). The activity of MazF is neutralized by the short-lived antitoxin MazE, which is degraded by the stress induced serine protease ClpPA. The antitoxin MazE protein consists of two domains: an N-terminal DNA binding domain that can regulate gene expression by binding to its own promoter and a C-terminal flexible end that can bind to MazF, impeding the endoribonuclease activity of MazF (Kamada et al., 2003, Loris et al., 2003, Kamphuis et al., 2006).

*Deinococcus radiodurans* is a gram-positive bacterium that is remarkably resistant to several types of stress, such as desiccation, oxidative stress and DNA damage by ionizing or ultraviolet radiation (Battista, Earl et al. 1999, Zahradka et al., 2006, Daly 2009). Several mechanisms have been proposed for its extreme resistance to radiations. The strong cell defense systems of *D. radiodurans* involving catalase and $Mn^{2+}$ dependent antioxidant enzymes such as superoxide dismutase protect its essential proteins such as DNA repair enzymes from oxidative damage (Slade and Radman 2011). In addition, an efficient DNA repair mechanism involving critical repair proteins like RecA and PPrI is essential for the recovery of a fully functional genome (Pavlopoulou et al., 2016). Otherwise, although several other survival mechanisms have been proposed, too little is understood about the role of the TA systems of *D. radiodurans* in cell survival. A recent report (Li et al., 2017) suggested that the locus *dr*0416-*dr*0417 of the *D. radiodurans* genome, which encodes a functional MazEF system, mediates the suicide of a sub-population and the survival of remaining population under DNA damage stress. This reported mechanism mimics that of *M. xanthus*, in which the MazF-mediated cell death of a subpopulation is required for the development of a multicellular fruiting body from the remaining population (Nariya and Inouye, 2008). This cell suicide behavior of a sub-population might favor bacteria in such a way that the remaining population becomes the seed when the external stresses are lessened, implying the importance of the regulation of TA protein expression for the sustainability of pathogenicity. However, little is known about the regulations of the TA proteins at the cellular and molecular levels. Therefore, to obtain a better understanding of the detailed molecular mechanism of the MazEF-mediated cell death pathway, we performed structural studies of the DrMazEF complex from *D. radiodurans*.

The genes *dr*0416 and *dr*0417, which correspond to DrMazE and DrMazF, were cloned into the plasmids pBAD33 and pET11akm-GST, respectively. DrMazE and DrMazF formed a complex *in vivo* when they were co-overexpressed in an *E. coli* expression system, and the resulting complex was then isolated, purified and crystallized.

A sequence based BLAST analysis revealed that the structure of *E. coli* MazF toxin (PDB: 3NFC) is the closest homolog of *D. radiodurans* MazF, with a sequence identity of 46%. Therefore, the structural model of *E. coli* MazF was used for molecular replacement in resolving the structure of the DrMazEF complex. Although a complex structure has already been reported for *E. coli* MazEF (PDB: 1UB4) that revealed the binding mechanisms of the toxin and its antidote protein, our structural study will reveal further insight into how MazF and MazE interact to induce the MazEF-mediated cell death pathway in *D. radiodurans*. Here, as a first step in determining the structure of DrMazEF complex, we report its cloning, purification, crystallization, and preliminary X-ray diffraction data.

## RESULTS AND DISCUSSION

The genes *dr*0416 and *dr*0417, which correspond to DrMazE (12 kDa) and DrMazF (9 kDa), were isolated and cloned into pBAD33 and pET11akm-GST, respectively. DrMazF with its N-terminal glutathione *S*-transferase (GST)-tag was toxic to the host cells when expressed alone. We therefore co-expressed the tagged toxin protein GST-DrMazF (38 kDa) together with its antidote DrMazE without a tag. Cells of *E. coli* BL21 (DE3) were transformed with the plasmids pBAD33-DrMazE and pET11akm-GST-DrMazF containing chloramphenicol and kanamycin resistance markers, respectively. Protein expression

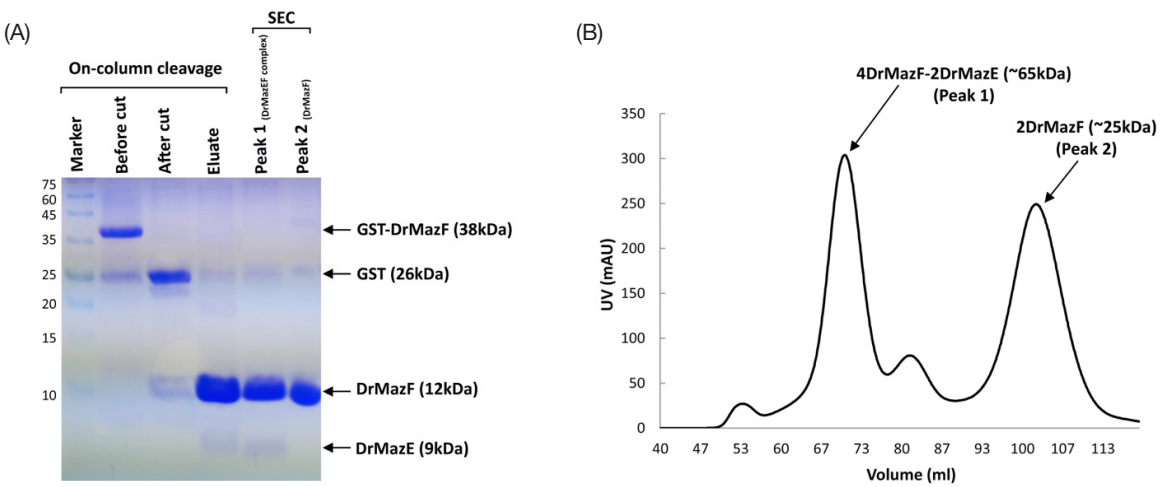


**FIGURE 1 | Purification of the Deinococcus radiodurans MazEF complex.** (A) On-coloumn cleavage and isolation of Glutathione *S*-transferase (GST)-DrMazEF. lane 1, protein marker; lanes 2–4, on-column cleavage of GST-DrMazF; lanes 5–6. Fractions from peaks 1 and 2 in (B) were concentrated and loaded. (B) DrMazEF complex and DrMazF were separated by size-exclusion chromatography using a Superdex™ 200 gel filtration column.

was induced using 0.2% L-arabinose and 0.1 mM isopropyl-β-D-thiogalactopyranoside (IPTG) for DrMazE and GST-DrMazF, respectively. The two proteins appeared to be stably expressed and formed a complex, although DrMazE could barely be detected on gel analysis due to its relatively small molecular weight (data not shown).

The cells containing the overexpressed proteins were lysed and centrifuged. The supernatant containing the soluble recombinant protein complex was passed through the glutathione Sepharose beads, which were then washed repeatedly to remove contaminants and purify the GST-DrMazF and GST-DrMazEF complex bound to the beads (Figure 1A, lane 1). The gel analysis results indicated that the fusion protein GST-DrMazF was properly folded and we were able to isolate the recombinant protein successfully.

GST-DrMazF contained a thrombin cleavage site, which we used to remove the GST tag. Upon on-column cleavage with thrombin, the flow-through elute was likely to contain DrMazEF complex with an excess amount of DrMazF (Figure 1A, lane 4), while the GST tag remained bound to the beads (Figure 1A, lane 3). The band in lane 4, corresponding to a molecular weight of 9 kDa, clearly reflects that the untagged DrMazE was able to form a stable complex with DrMazF *in vivo* during their co-expression.

The flow-through eluate containing the proteins of interest was concentrated and purified using a size-exclusion chromatography to separate the excess DrMazF and DrMazEF complex (Figure 1A, lanes 5 and 6). The size-exclusion chromatography analysis of the eluate showed two peaks corresponding to approximately 65 kDa and 25 kDa (Figure 1B). An analysis by sodium dodecyl sulfate-polyacrylamide gel electrophoresis showed that the fractions from the peak 1 showed two bands at approximately at 9 kDa and 12 kDa, while peak 2 had one band at approximately at 12 kDa (Figure 1A, lanes 5 and 6). Hence, we concluded that peak 1 corresponds to the DrMazEF heterohexamer based on combinatorial molecular weight estimations, while peak 2 corresponds to the DrMazF homodimer. These findings

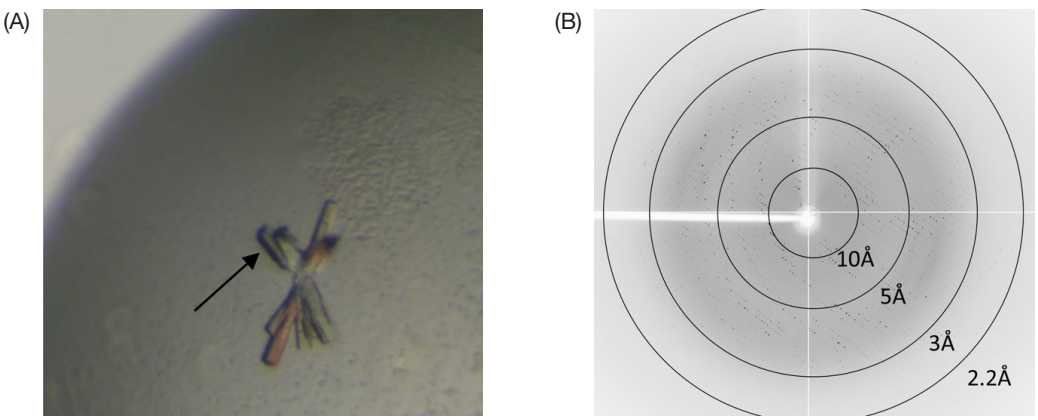


**FIGURE 2 | Crystallization and diffraction.** (A) Crystal cluster of the DrMazEF complex. Crystals with smooth edges were obtained using the hanging drop vapor-diffusion method at 20 °C. (B) X-ray diffraction image of the *D. radiodurans* MazEF complex crystal. The crystal was diffracted to a resolution of 2.6 Å on beamline 7A at the Pohang Accelerator Laboratory, Pohang, South Korea.

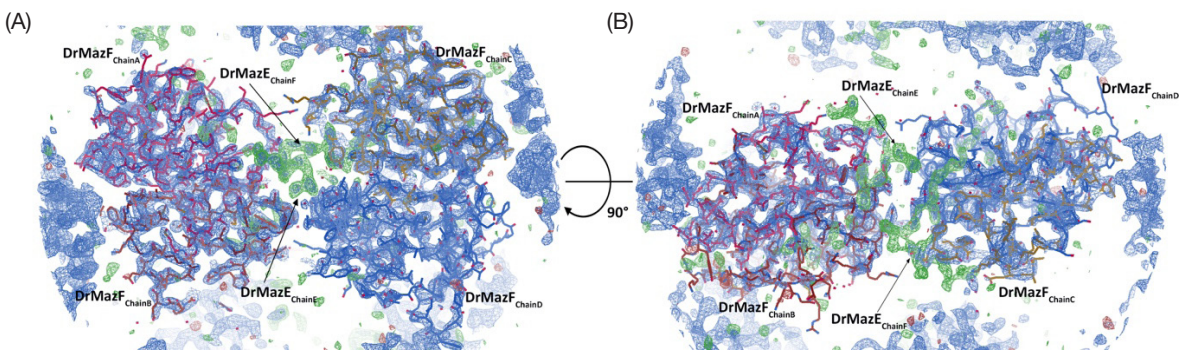


**FIGURE 3 | Electron density maps generated by molecular replacement phasing revealed the presence of DrMazE.** (A) and (B) Initial $2F_o$-$F_c$ maps (blue) contoured at 1.5σ after phasing revealed the DrMazF backbone with a perfect fit and $F_o$-$F_c$ maps (green) revealed a clear electron density map for DrMazE. The amino acid sequences of DrMazE were manually fit according to the map using *Coot*.

**TABLE 1** | Crystallographic data collection statistics for the DrMazEF complex

| Diffraction statistics | DrMazEF |
|---|---|
| Beamline | PAL-7A |
| Wavelength (Å) | 0.97934 |
| Temperature (K) | 100 |
| Detector | ADSC Quantum Q270 |
| Crystal detector distance (mm) | 270 |
| Total rotation range (°) | 1 |
| Space group | 360 |
| Cell parameters | $P2_12_12_1$ |
| *a, b, c* (Å) | 46.01, 74.04, 138.26 |
| *α, β, γ* (°) | 90.0, 90.0, 90.0 |
| Data resolution (Å) | 50.0 – 2.6 (29.81 – 2.612) |
| Completeness (%) | 99.5 (65.7) |
| Redundancy | 9.3 (8.6) |
| Total reflection | 128972 |
| Unique reflections | 13627 (976) |
| $R_{merge}$* (%) | 12 (52.4) |
| Average I/σ (I) | 23.6 (18.8) |
| Matthew's coefficient ($Å^3$ $Da^{-1}$) | 1.84 |
| Solvent content (%) | 33.18 |
| No. of chains per asymmetric unit | 6 |

Values in parentheses correspond to the highest resolution shell
* $R_{merge}=\Sigma_{hkl}\ \Sigma_i\ |I_i(hkl) - <I(hkl)>| / \Sigma_{hkl}\ \Sigma_i\ I_i(hkl)$, where $I_i(hkl)$ and $<I(hkl)>$ are the intensity of an individual reflection and the mean value of all measurements of anindividual reflection, respectively.

reaffirmed that the DrMazEF complex exists in a heterohexameric (2MazF-2MazE-2MazF) state in solution, similar to EcMazEF and MtMazE. The fractions from peak 1 corresponding to the DrMazEF complex were then concentrated and subjected to crystallization trials using the hanging drop method.

Amongst the screening kits mentioned in the materials and methods section, only one condition (Index 40; 100 mM citric acid [pH 3.5] and 25% PEG3350) yielded a crystal after 1 month of incubation at 20°C (Figure 2A). The protein complex was resistant to crystallization owing to the fact that DrMazE is highly flexible and labile protein according to the secondary structural analysis (https://npsa-prabi.ibcp.fr/cgi-bin/secpred_gor4.pl). This crystal with improved quality was soaked in a cryoprotectant solution containing the well solution and 15% glycerol. The crystal was then flash frozen using liquid nitrogen for diffraction.

The crystal diffracted to a resolution of 2.6 Å (Figure 2B) with reliable diffraction statistics (Table 1). Based on the auto-indexing and scaling using *HKL-2000*, the crystal belonged to the space group $P2_12_12_1$, with the unit cell parameters a = 46.01, b = 74.04, c = 138.26Å, and α=β=γ= 90° (Table 1). A total of 128,972 reflections were measured in the range of 50.0-2.6Å. The asymmetric unit of the crystal had six molecules in two heterotrimeric complex (2DrMazF-DrMazE), with a calculated Mathew's coefficient of 1.84 $Å^3$ $Da^{-1}$ and a solvent content of 33.18% (Matthews, 1968).

We attempted to solve the structure by molecular replacement using the single chain of the EcMazF toxin (PDB: 3NFC) as a search model, since this protein exhibits a high levels of sequence identity to DrMazF (46%). The initial round of crystallographic refinement using the best model obtained by molecular replacement was subjected to rigid-body refinement, resulting in convergence to an R factor of 39.45% and an $R_{free}$ of 46.65% with four chains of DrMazF in the asymmetric unit. A clearly distinguishable $F_o$-$F_c$ map was seen to correspond to the DrMazE protein (Figure 3). The model was built according to the map using *Coot* (Emsley and Cowtan 2004) and following several rounds of refinement cycles, the R factor and $R_{free}$ were brought down to 24.83% and 29.37% respectively. Further refinement is in progress to complete the quaternary structure of the stable DrMazEF complex.

## METHODS

### Plasmid constructs and culture condition

The two genes of interest *dr*0416 and *dr*0417, which correspond to DrMazE and DrMazF, were cloned into the plasmids pBAD33 (forward primer: Nde1-**CATATG**ACGAGTCAAATTCAG; reverse primer: BamH1-**GGATCC**TTACCATTCCTCGCG) and pET11akm-GST (forward primer: Nde1- **CATATG**GTAAGCGATTATGTC; reverse primer: BamH1-**GGATCC**TCATGCCTTCTCGGA), respectively. The plasmids pBAD33 and pET11akm-GST contained the antibiotic resistance markers for chloramphenicol and kanamycin, respectively. For the expression of the recombinant enzyme, *E. coli* BL21 (DE3) cells transformed with pBAD33-*dr*0416 (DrMazE) and pET11akm-GST-*dr*0417 (DrMazF) were grown in Luria-Bertani (LB) medium (1 L) containing 100 µg/mL kanamycin and chloramphenicol at 37°C to the mid-exponential phase ($A_{600}$ = 0.6). After induction by 0.2% L-arabinose and 1 mM of isopropyl-β-D-thiogalactopyranoside (IPTG) for DrMazE and DrMazF, respectively, the cells were grown for an additional 6 hours at 37°C and harvested by centrifugation (10,000 × g, 20 min, 4°C). The bacterial pellets were stored at -20°C.

### DrMazEF complex isolation and purification

The frozen bacterial pellets were resuspended in lysis buffer (50 mM Tris-HCl, 150 mM NaCl, 1 mM dithiothreitol and 1 mM phenylmethylsulfonyl fluoride; pH 8.0) and disrupted by sonication (Pulse: 20-s intervals, 35% amplitude). The lysate was centrifuged at 20,000 × g for 30 min to remove the cell debris. The filtrate was applied to a glutathione Sepharose™ 4B bead (GE healthcare, Little Chalfont, UK) equilibrated with the lysis buffer. The column was washed with the same lysis buffer followed by cleavage buffer (20 mM Tris HCl pH 7.5, 150 mM NaCl). For an on-column cleavage, to remove the GST tag from the DrMazF protein, human α-thrombin (Haematologic Technologies Inc., Essex, VT) was added at a 1:5000 ratio (enzyme:buffer) and incubated overnight at 4°C for cutting the GST tag from DrMazF protein while circulating the thrombin-containing buffer at a speed of 2 mL/min. After cleavage, the reaction was stopped by adding 1 mM phenylmethylsulfonyl fluoride, and the flow-through eluate contained the DrMazEF complex and an excess of DrMazF while the GST tag remained bound to the bead. The pooled fractions were then subjected to size-exclusion chromatography on a HiLoad™ 16/600 Superdex™ 200 column (GE Healthcare, USA) equilibrated with crystallization buffer (20 mM Tris-HCl pH 7.5, 50 mM NaCl). The fractions from peak 2

corresponding to the DrMazEF complex were mixed and concentrated for crystallization.

### Crystallization

The purified DrMazEF complex was concentrated to 7-10 mg/mL in crystallization buffer using a concentrator (Millipore, Billerica, MA). Hanging-drop vapor diffusion crystallization trials using 1 $\mu$L of protein and 1 $\mu$L of reservoir solution were performed on a 24well VDX plate (Hampton Research, Aliso Viejo, CA) using kits from Hampton Research (Index, SaltRx, PEG/Ion, PEG/Ion 2, Crystal Screen, Crystal Screen 2, and Crystal Screen Lite, USA) and Emerald Biosystems kits (Wizard I, II, III and IV, Bainbridge Island, WA). Crystals of the DrMazEF complex formed from Index 40 (100 mM citric acid [pH 3.5] and 25% PEG3350) after 1 month of incubation at 20°C (Figure 2A). Crystal clusters were initially formed from this condition. Hence, one smooth edged crystal was carefully broken and separated from the cluster using a Micro-Scraper (Hampton Research, USA). That crystal was then soaked for 30 s in cryoprotectant (containing the well solution and 15% glycerol) and then cooled in liquid nitrogen for synchrotron-radiation diffraction.

### X-ray crystallography

The crystals of the DrMazEF complex were subjected to diffraction using beamline 7A at the Pohang Accelerator Laboratory (Pohang, Korea). X-ray diffraction was performed at 100K in a cryogenic $N_2$ gas stream with an oscillation of 1.0° for 1 s exposure over a 360° range. The crystal was diffracted to a resolution of 2.6 Å and belonged to the space group $P2_12_12_1$ (Table 3). Data were processed and scaled with *HKL-2000* (Otwinowski and Minor 1997) and the diffraction statistics are listed in Table 1. The data analysis showed that the crystal had a solvent content of 33.18 % and a Matthews coefficient of 1.84 $Å^3$ $Da^{-1}$. We solved the structure by molecular replacement using the single chain of MazF toxin from *E.coli* as a search model (PDB entry 3NFC), which exhibits high levels of sequence identity and similarity of 46% and 60% respectively, to DrMazF toxin. With a good molecular-replacement solution, an initial round of crystallographic refinement was carried out using rigid-body refinement, resulting in convergence to an R factor of 39.45% and $R_{free}$ of 46.65% with 4 chains of DrMazF and 2 chains of unbuilt DrMazE in the asymmetric unit (Figure 3). The amino acids of the chains were manually replaced and built using *coot* (Emsley and Cowtan 2004).

## CONFLICT OF INTEREST

The authors declare that they have no conflict of interest.

## ACKNOWLEDGEMENTS

We thank the staff members of the Pohang Accelerator Laboratory beamline 7A for their help with data collection. This work was supported by a research fund from Chosun University, 2017.

Original Submission: Jan 15, 2018
Revised Version Received: Mar 12, 2018
Accepted: Mar 12, 2018

## REFERENCES

Aakre, C.D., Phung, T.N., Huang, D., and Laub, M.T. (2013). A bacterial toxin inhibits DNA replication elongation through a direct interaction with the beta sliding clamp. *Mol Cell* **52**, 617-628.

Aizenman, E., Engelberg-Kulka, H., and Glaser, G. (1996). An Escherichia coli chromosomal "addiction module" regulated by guanosine [corrected] 3',5'-bispyrophosphate: a model for programmed bacterial cell death. *Proc Natl Acad Sci U S A* **93**, 6059-6063.

Battista, J.R., Earl, A.M., and Park, M.J. (1999). Why is Deinococcus radiodurans so resistant to ionizing radiation? *Trends Microbiol* **7**, 362-365.

Daly, M.J. (2009). A new perspective on radiation resistance based on Deinococcus radiodurans. *Nat Rev Microbiol* **7**, 237-245.

Emsley, P., and Cowtan, K. (2004). Coot: model-building tools for molecular graphics. *Acta Crystallogr D Biol Crystallogr* **60**, 2126-2132.

Gerdes, K., Christensen, S.K., and Lobner-Olesen, A. (2005). Prokaryotic toxin-antitoxin stress response loci. *Nat Rev Microbiol* **3**, 371-382.

Kamada, K., Hanaoka, F., and Burley, S.K. (2003). Crystal structure of the MazE/MazF complex: molecular bases of antidote-toxin recognition. *Mol Cell* **11**, 875-884.

Kamphuis, M.B., Bonvin, A.M., Monti, M.C., Lemonnier, M., Munoz-Gomez, A., van den Heuvel, R.H., Diaz-Orejas, R., and Boelens, R. (2006). Model for RNA binding and the catalytic site of the RNase Kid of the bacterial parD toxin-antitoxin system. *J Mol Biol* **357**, 115-126.

Li, T., Weng, Y., Ma, X., Tian, B., Dai, S., Jin, Y., Liu, M., Li, J., Yu, J., and Hua, Y. (2017). Deinococcus radiodurans Toxin-Antitoxin MazEF-dr Mediates Cell Death in Response to DNA Damage Stress. *Front Microbiol* **8**, 1427.

Loris, R., Marianovsky, I., Lah, J., Laeremans, T., Engelberg-Kulka, H., Glaser, G., Muyldermans, S., and Wyns, L. (2003). Crystal structure of the intrinsically flexible addiction antidote MazE. *J Biol Chem* **278**, 28252-28257.

Makarova, K.S., Wolf, Y.I., and Koonin, E.V. (2009). Comprehensive comparative-genomic analysis of type 2 toxin-antitoxin systems and related mobile stress response systems in prokaryotes. *Biol Direct* **4**, 19.

Masuda, Y., Miyakawa, K., Nishimura, Y., and Ohtsubo, E. (1993). chpA and chpB, Escherichia coli chromosomal homologs of the pem locus responsible for stable maintenance of plasmid R100. *J Bacteriol* **175**, 6850-6856.

Nariya, H., and Inouye, M. (2008). MazF, an mRNA interferase, mediates programmed cell death during multicellular Myxococcus development. *Cell* **132**, 55-66.

Otwinowski, Z., and Minor, W. (1997). Processing of X-ray diffraction data collected in oscillation mode. *Methods Enzymol* **276**, 307-326.

Pavlopoulou, A., Savva, G.D., Louka, M., Bagos, P.G., Vorgias, C.E., Michalopoulos, I., and Georgakilas, A.G. (2016). Unraveling the mechanisms of extreme radioresistance in prokaryotes: Lessons from nature. *Mutat Res Rev Mutat Res* **767**, 92-107.

Slade, D., and Radman, M. (2011). Oxidative stress resistance in Deinococcus radiodurans. *Microbiol Mol Biol Rev* **75**, 133-191.

Tsuchimoto, S., Ohtsubo, H., and Ohtsubo, E. (1988). Two genes, pemK and pemI, responsible for stable maintenance of resistance plasmid R100. *J Bacteriol* **170**, 1461-1466.

Wang, X., and Wood, T.K. (2011). Toxin-antitoxin systems influence biofilm and persister cell formation and the general stress response. *Appl Environ Microbiol* **77**, 5577-5583.

Zahradka, K., Slade, D., Bailone, A., Sommer, S., Averbeck, D., Petranovic, M., Lindner, A.B., and Radman, M. (2006). Reassembly of shattered chromosomes in Deinococcus radiodurans. *Nature* **443**, 569-573.